

Giant Second Harmonic Generation from Wafer-Scale Aligned Chiral Carbon Nanotubes

Rui Xu^{1†}, Jacques Doumani^{2,3†}, Viktor Labuntsov⁴, Nina Hong⁵, Anna-Christina Samaha^{6,7}, Weiran Tu¹, Fuyang Tay^{2,3}, Elizabeth Blackert¹, Jiaming Luo^{1,3}, Mario El Tahchi^{6,7}, Weilu Gao⁸, Jun Lou¹, Yohei Yomogida⁹, Kazuhiro Yanagi⁹, Riichiro Saito^{9,10,11}, Vasili Perebeinos^{4*}, Andrey Baydin^{2,12*}, Junichiro Kono^{1,2,12,13*} and Hanyu Zhu^{1,2,12,13*}

¹Department of Materials Science and NanoEngineering, Rice University, Houston, 77005, Texas, USA.

²Department of Electrical and Computer Engineering, Rice University, Houston, 77005, Texas, USA.

³Applied Physics Graduate Program, Smalley-Curl Institute, Rice University, Houston, 77005, Texas, USA.

⁴Department of Electrical Engineering, University at Buffalo, Buffalo, 14228, New York, USA.

⁵J.A. Woollam Co., Inc., Lincoln, 68508, Nebraska, USA.

⁶Laboratory of Biomaterials and Intelligent Materials, Lebanese University, Jdeidet, 90656, Lebanon.

⁷Department of Physics, Lebanese University, Jdeidet, 90656, Lebanon.

⁸Department of Electrical and Computer Engineering, University of Utah, Salt Lake City, 84112, Utah, USA.

⁹Department of Physics, Tokyo Metropolitan University, Tokyo, 192-0397, Japan.

¹⁰Department of Physics, Tohoku University, Sendai, 980-8578, Japan.

¹¹Department of Physics, National Taiwan Normal University, Taipei, 106, Taiwan.

¹²Smalley-Curl Institute, Rice University, Houston, 77005, Texas, USA.

¹³Department of Physics and Astronomy, Rice University,
Houston, 77005, Texas, USA.

*Corresponding author(s). E-mail(s): vasilipe@buffalo.edu;
baydin@rice.edu; kono@rice.edu; hz67@rice.edu;

Contributing authors: rx8@rice.edu; jd74@rice.edu;
labuntsov99@mail.ru; nhong@jawoollam.com;
annachristina.samaha@st.ul.edu.lb; wt20@rice.edu; ft13@rice.edu;
erb13@rice.edu; jl230@rice.edu; mtahchi@ul.edu.lb;
weilu.gao@utah.edu; jlou@rice.edu; yomogida@tmu.ac.jp;
yanagi-kazuhiro@tmu.ac.jp; rsaito@tohoku.ac.jp;

†These authors contributed equally to this work.

Abstract

Chiral carbon nanotubes (CNTs) are direct-gap semiconductors with optical properties governed by one-dimensional excitons with enormous oscillator strengths. Each species of chiral CNTs has an enantiomeric pair of left- and right-handed CNTs with nearly identical properties, but enantiomer-dependent phenomena can emerge, especially in nonlinear optical processes. Theoretical studies have predicted strong second-order nonlinearities for chiral CNTs, but there has been no experimental verification due to the lack of macroscopically ordered assemblies of single-enantiomer chiral CNTs. Here for the first time, we report the synthesis of centimeter-scale films of densely packed and aligned single-enantiomer chiral CNTs that exhibit micro-fabrication compatibility. We observe giant second harmonic generation (SHG) emission from the chiral CNT film, which originates from the intrinsic chirality and inversion symmetry breaking of the atomic structure of chiral CNTs. The observed value of the dominant element of the second-order nonlinear optical susceptibility tensor reaches 1.5×10^3 pm/V at a pump wavelength of 1030 nm, corresponding to the lowest-energy excitonic resonance. Our calculations based on many-body theory correctly estimate the spectrum and magnitude of such excitonically enhanced optical nonlinearity. These results are promising for developing scalable chiral-CNT electronics, nonlinear photonics and photonic quantum computing.

Main Text

Structural chirality is a fundamental property in which the material is not identical to its mirror image. Materials possessing chirality can enable intriguing properties, including optical activity [1, 2], magneto-chiral effects [3, 4], and chiral-induced spin selectivity [5, 6], which can be useful for information

processing and transfer applications [7–10]. Due to lifted inversion symmetry in chiral materials, second-order optical nonlinearity is also expected for conventional chiral crystalline insulators including α -quartz and TeO_2 [11, 12] and recently discovered chiral semiconductors such as hybrid organic-inorganic halides [13–15], with resonance-enhanced nonlinear optical susceptibilities $\chi^{(2)}$ of up to 100 pm/V. However, it is counter-intuitive that second harmonic generation (SHG) can arise purely from structural chirality without any local electrical or magnetic polarization, such as in non-magnetic elemental allotropes. Indeed, Kleinman symmetry dictates that SHG is forbidden in isotropic chiral materials without dispersions [16]. Previously, crystalline anisotropy and large dispersions have enabled large SHG from tellurium, a chiral elemental allotrope [17–19], but the nonlinear susceptibility was only quantified at far-infrared wavelengths, instead of near the resonance at the bandgap [20].

Chiral carbon nanotubes (CNTs) are ideal candidates for exploring chirality-induced nonlinear optical phenomena. Since their discovery, CNTs have shown unique electronic, photonic, and mechanical properties arising from one-dimensional (1D) quantum confinement effects [21–24]. Calculations have predicted strong 1D van Hove singularity-enhanced second-order nonlinearities, $\chi^{(2)}$ on the order of nm/V, for chiral species of single-wall CNTs, where their chirality indices (n, m) satisfy $n \neq m$ and $m \neq 0$ [25, 26]. Such chiral CNTs are semiconductors with diameter (d_t)-dependent direct band gaps [27], E_g (eV) $\sim 0.7/d_t$ (nm), potentially useful for integrated nanophotonics and chiral optoelectronics. Being 1D semiconductors with $d_t \sim 1$ nm, chiral CNTs exhibit enormous excitonic effects, which can resonantly boost SHG processes further [28]. Several experiments have observed SHG from different types of CNT materials, including single tubes [29], thin films [30, 31], and chiral CNTs embedded in host porous crystals [32]. However, the observed optical nonlinearity was very weak (effective $\chi^{(2)} \sim 0.01$ pm/V) due to the coexistence of both enantiomers, random CNT orientations, and low packaging densities, hindering both fundamental studies and practical applications. Furthermore, the observed SHG may have originated from surface effects or local defects instead of the intrinsic chirality of CNTs since the symmetry of the observed signal disagreed with the expected SHG tensor of chiral CNTs, which should contain only two non-zero elements, i.e., $\chi_{xyz}^{(2)}$ and $\chi_{yxz}^{(2)}$ ($= -\chi_{xyz}^{(2)}$).

Here, we report the fabrication of centimeter-scale films of aligned enantiomer-pure chiral CNTs and the observation of giant SHG from the films. We chose $(6,5)^-$ CNTs for this study; $(6,5)^+$ and $(6,5)^-$ are the left-handed and right-handed enantiomers, respectively, of the otherwise identical CNT species with $d_t = 0.76$ nm and $E_g \sim 1$ eV. Incident angle- and polarization-dependent measurements of SHG, combined with analysis of the $\chi^{(2)}$ tensor, confirmed that the observed SHG signal originated from the intrinsic structural chirality of the $(6,5)^-$ CNTs. The excitation-wavelength-dependence of the SHG signal exhibited a prominent peak at around the E_{11} exciton resonance ($\sim 1 \mu\text{m}$), in agreement with the results of our calculations based on

many-body theory. Excitation power dependence showed a deviation from the expected quadratic behavior for excitation intensities above a threshold of $\sim 0.2 \text{ mJ/cm}^2$, which we attribute to absorption saturation due to exciton-exciton annihilation [33]. From the measured SHG signals, we estimated the value of $\chi_{xyz}^{(2)}$ to be $1.5 \times 10^3 \text{ pm/V}$, which is comparable with values reported for single-crystalline two-dimensional semiconductors and Weyl semimetals [34–38]. These results demonstrate that aligned enantiomer-pure CNT films, which can be easily transferred to any substrate with excellent conformity and scalability, are promising for applications in integrated chiral nano-photonics and chiral quantum optics [39].

We first prepared an aqueous suspension of enantiomer-enriched $(6,5)^-$ CNTs and measured its enantiomer purity (EP). The suspension was purified using gel chromatography [40–42], as illustrated in Fig. 1a and described in more detail in Methods. The EP of the suspension was characterized by circular dichroism (CD) spectroscopy; see Fig. 1b. The CD intensity spectrum exhibits multiple peaks corresponding to the E_{ij} excitonic transitions shown in the attenuation spectrum; here, i and j are integers, and transitions with $i = j$ are strongly allowed for light polarization parallel to the nanotube axis [43]. The EP of the $(6,5)^-$ CNT suspension can be calculated from the CD intensity (in mdeg) normalized by the attenuance A at the E_{22} transition, denoted by $CD_{E_{22}}$ and $A_{E_{22}}$, respectively, as follows [44]:

$$EP(6,5)^- = \left(50 - 0.421 \frac{CD_{E_{22}}}{A_{E_{22}}} \right) \% = 91.6\%, \quad (1)$$

where we used $CD_{E_{22}} = -29.67 \text{ mdeg}$ and $A_{E_{22}} = 0.30$; see Supporting Information Section 1 for zoom-in data. This EP value is comparable with the state-of-art in the literature [45].

We then fabricated three CNT films using the CVF method [46] and transferred them onto fused silica substrates (Fig. 1c and Methods). The first film, labeled ‘chiral aligned’ or CA, contained aligned enantiomer-pure $(6,5)^-$ CNTs. The film preserved the single-chirality nature of the original CNT suspension, as evidenced by Raman spectra (Supporting Information Section 1) [47]. The second sample, labeled ‘chiral random’ or CR, contained randomly oriented enantiomer-pure $(6,5)^-$ CNTs prepared from the same suspension as the CA film. Finally, the third film, labeled ‘racemic aligned’ or RA, consisted of highly aligned CNTs containing metallic and semiconducting CNTs with mixed chiralities [46]. All three films had the same thickness of around 20 nm, measured by atomic force microscopy (Supporting Information Section 2). Scanning electron microscope images indicated that these films were densely packed with CNTs with no visible voids at optical wavelength scales (Fig. 1d and Supporting information Section 3).

Polarized attenuance spectra for the CA film (Fig. 1f) confirmed its global in-plane anisotropy within a probed area of $1.2 \times 10^3 \mu\text{m}^2$. The first three peaks in the attenuance spectra correspond to the E_{11} exciton resonance

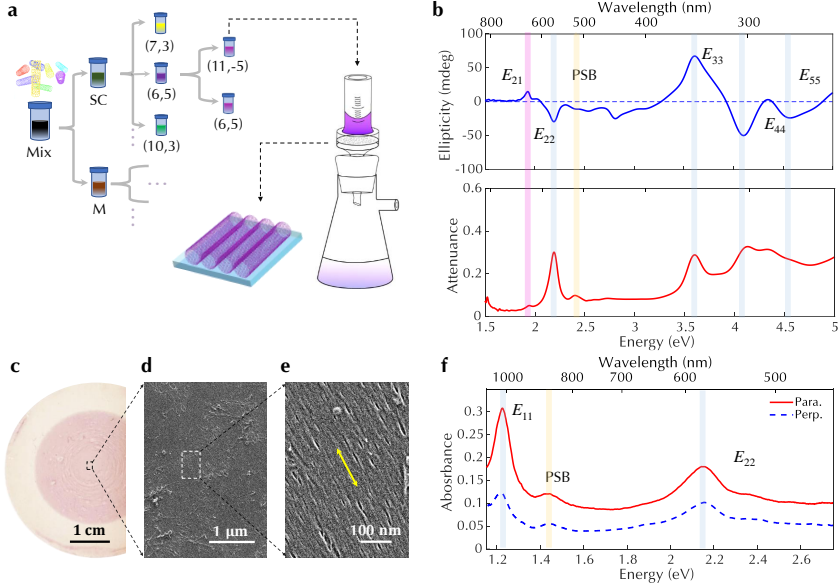


Fig. 1 Fabrication and characterization of an aligned film of enantiomer-pure (6,5)⁻ CNTs. **a**, An as-purchased mixture of CNTs was dispersed in water and separated by their metallicity and chirality via multi-step gel chromatography. A (6,5)⁻ CNT suspension was extracted, and an aligned film was made by using controlled vacuum filtration (CVF); the fabricated film was transferred onto a fused silica substrate. **b**, Circular dichroism and attenuation spectra for the (6,5)⁻ CNT suspension. Analysis of these spectra yielded an enantiomer purity of 91.6%. **c**, An optical image of the chiral aligned (CA) CNT thin film with a diameter of 3 cm. **d,e**, SEM images of CA CNT thin film at low and high magnifications, respectively, demonstrating the film's uniformity, high packing density, and microscopic in-plane anisotropy. The yellow arrow indicates the alignment direction. **f**, Global linearly polarized attenuation spectra for the CA sample with a probed area of about $1.2 \times 10^3 \mu\text{m}^2$. The observed peaks are due to the E_{11} exciton resonance, the E_{11} exciton phonon sideband (PSB), and the E_{22} exciton resonance. The linear dichroism value at E_{11} is 0.9, corresponding to a nematic order parameter of ~ 0.45 .

(1.23 eV), the phonon sideband of the E_{11} exciton resonance (PSB, 1.43 eV), and the E_{22} exciton resonance (2.15 eV), respectively. The difference in E_{11} attenuation between parallel (A_H) and perpendicular (A_V) polarizations with respect to the CNT alignment direction yields a linear dichroism (LD) of $2 \times (A_H - A_V)/(A_H + A_V) = 0.9$, corresponding to a nematic order parameter $S = 0.45$ within the probed area [48]. On a more local scale within an optically resolvable area of $1.3 \mu\text{m}^2$, the CA film showed stronger alignment with $S = 0.66 \sim 0.71$ (Supporting Information Section 4). The random orientation of CNTs in the CR film was also confirmed ($S = 0.04$) by its lack of LD (Supporting Information Section 5) as well as SEM images (Supporting Information Section 3).

Next, we resonantly pumped the CA film in the vicinity of E_{11} exciton transition energy ($\sim 1.2\text{eV}$) and measured emitted radiation at the second

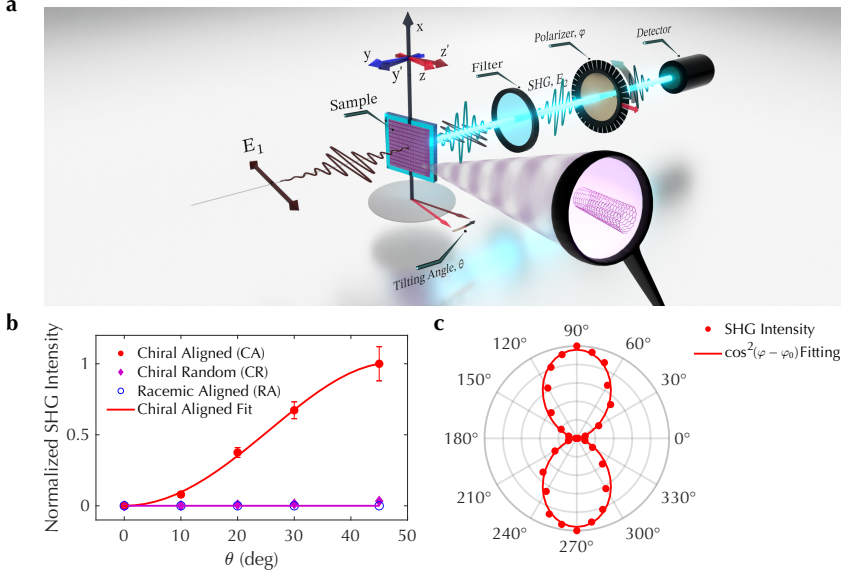


Fig. 2 Quantifying the SHG tensor elements of aligned enantiomer-pure $(6,5)^-$ CNT thin films. **a**, The excitation pulse is horizontally polarized (z -axis), whose electric field is at an angle θ with respect to the CNT alignment direction. The emitted SHG is separated from the excitation pulse by an optical filter and analyzed via a polarizer at an angle φ from the excitation polarization. Axes with (without) the prime denote the lab (sample) coordinate system. Inset shows the chiral atomic structure of a single $(6,5)^-$, a left-handed CNT. **b**, Strong SHG emission is observed in the chiral enantiomer-pure and aligned (CA) film under non-zero tilting angle, as expected from the $\chi_{yxz}^{(2)}$ element, compared with negligible SHG from either the chiral random (CR) or racemic aligned (RA) films. **c**, The emitted SHG radiation is vertically polarized, which is orthogonal to the excitation pulses, again in agreement with the symmetry of the SHG tensor. Here, the fitting parameter φ_0 is the angle between the SHG polarization and the z axis in the laboratory system.

harmonic ($\sim 2.4\text{ eV}$). In chiral CNTs, such as $(6,5)$ CNTs, only one independent nonzero element, $\chi_{x'y'z'}^{(2)} = -\chi_{y'x'z'}^{(2)}$, exists in the second order nonlinear optical susceptibility tensor [25], where z' denotes the nanotube axis in the sample coordinate system (Fig. 2a and Supporting Information Section 7). Therefore, the intensity of SHG, I_{SHG} , arising from the intrinsic structural chirality should be nonzero only when the electric field of the incident light has finite projections onto both the y' and z' axes in the sample coordinate system:

$$I_{\text{SHG}} \propto P_{x'}^2 = \left(2|\chi_{x'y'z'}^{(2)}| S E_{y'} E_{z'} \right)^2, \quad (2)$$

where S is the nematic order parameter of the film, $E_{y'}$ and $E_{z'}$ are the electric field projections of the fundamental field onto the y' and z' axes, respectively. The emission dipole $P_{x'}$ is expected to be linearly polarized along the x' axis (Supporting Information Section 7). As illustrated in Fig. 2a, the CNT film was initially aligned with the polarization of the fundamental beam

along the z -axis in the laboratory coordinate system and then tilted around the x -axis by an angle θ (Methods and Supporting Information Section 12). We observed strong SHG emission only from the CA film only when $\theta \neq 0^\circ$; under normal incidence ($\theta = 0^\circ$), no SHG was observed due to the absence of $E_{y'}$, as expected from Eq. 2. The angular dependence of the SHG emission intensity can be fit well by Eq.S17, which includes the effects of refraction and phase matching. At $\theta = 45^\circ$, we further confirmed that the polarization of the SHG radiation can be fit by $\cos^2(\varphi - \varphi_0)$, where φ_0 is the angle between the SHG polarization and the z axis in the laboratory system. As shown in Fig. 2c, we used φ_0 as a fitting parameter and obtained $\varphi_0 = 87.5^\circ$ as the optimum value, indicating that the SHG emission is vertically polarized along the x' (x) axis in the sample (laboratory) coordinate system, consistent with Eq. 2. The combined tilting angle- and polarization-dependent measurements provided strong evidence that the observed SHG signal stems from the intrinsic chirality of the CNTs instead of surface symmetry breaking, which should yield y' -polarized emission, or local defects in the film, which should give a finite SHG signal under normal incidence. We observed small nonzero SHG from the CR film with an intensity less than 3% of that from the CA film, likely due to a finite nematic order through local spontaneous alignment. We observed no SHG emission from the RA film within the detection limit. These results highlight the essential role of both enantiomer purity and alignment for observing strong SHG emission from films of chiral CNTs.

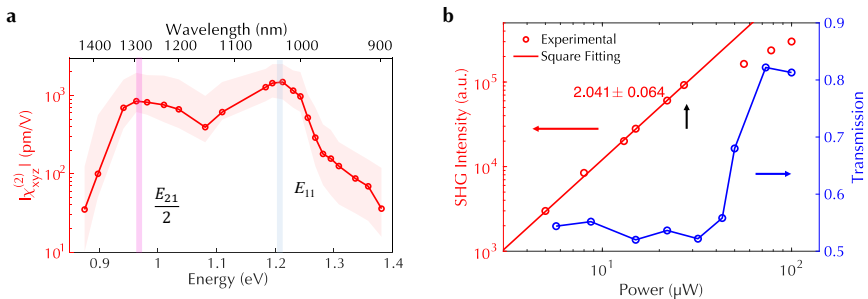


Fig. 3 Photon-energy and fluence dependence of the observed second-order optical nonlinearity of the aligned enantiomer-pure $(6,5)^-$ CNT film. **a**, Experimentally determined $|\chi_{xyz}^{(2)}|$ with a peak value approaching 1500 pm/V for excitation photon energy at around 1.2 eV near the E_{11} exciton resonance (blue shade) and an additional peak at around 1 eV near half of the E_{12} exciton resonance (purple shade), after correcting for the effects of multiple reflections, phase mismatch, CNT misalignment, and the collection efficiency of the setup. The width of the red-shaded area corresponds to the error range. **b**, The excitation fluence dependence of the SHG intensity (left axis) measured at a fundamental photon energy of 1.23 eV. The data shows a deviation from a quadratic fit above the saturation absorption threshold of ~ 0.2 mJ/cm² determined by power-dependent optical transmission measurements (right axis). The black arrow marks the excitation fluence used for taking the data shown in Fig. 3a, below which the SHG intensity exhibits a power-law dependence on the fluence with an optimum exponent of 2.04 ± 0.06 .

We determined the value of $|\chi_{xyz}^{(2)}|$ from the SHG data for the CA film as a function of excitation photon energy in the range between 0.87 eV and 1.37 eV, finding strong excitonic enhancement (Figure 3a). In quantifying $|\chi_{xyz}^{(2)}|$, we considered multiple reflections, phase mismatch, CNT misalignment, and the collection efficiency of the setup (Supporting Information Section 7). The spectrum shows a prominent peak centered at 1.21 eV, closely matching the absorption resonance of the E_{11} exciton observed in the linear optical susceptibility $|\chi_z^{(1)}|$ obtained through ellipsometry measurements (Supporting Information Section 8). The additional peak centered at 0.96 eV is attributed to the emission resonance with E_{12} exciton (Figure 1b), whose optical dipole is in the xy plane instead (Supplementary Information Section 9). The maximum measured $\chi_{xyz}^{(2)}$ is 1.5×10^3 pm/V, which is the largest experimentally verified value in any 1D material systems, to the best of our knowledge, and is comparable with the highest $\chi^{(2)}$ values in the near-infrared region reported for any other nonlinear optical materials [49–51].

We further performed excitation fluence dependent measurements. The intensity of SHG emission from the CA film (red curve, left axis in Fig. 3b) increased quadratically as a function of excitation fluence F_{pump} . In the small-fluence region, with F_{pump} values up to 0.12 mJ/cm², the data exhibited a power-law dependence with an optimum exponent $k = 2.04 \pm 0.06$ when fit by the function $I_{\text{SHG}} = AF_{\text{pump}}^k$, as expected for SHG. However, as F_{pump} was further increased, a deviation from the quadratic dependence was observed. The deviation started at $F_{\text{pump}} \sim 0.2$ mJ/cm², which coincided with the onset of saturation absorption measured by power-dependent transmission (blue curve, right axis in Fig. 3b). Such saturation behavior is commonly seen in CNT assemblies [52], but the observed threshold fluence for the CA film was larger by one order of magnitude than what was previously reported in randomly oriented semiconducting CNT films containing multiple chiralities [53]. This demonstrates that an aligned, densely packed, and enantiomer-pure CNT film is a more robust optical material. The data shown in Figures 2 and 3a were acquired by keeping F_{pump} below 0.12 mJ/cm² (marked by a black arrow in Fig. 3b) to stay in the quadratic regime.

Finally, we offer a comprehensive theoretical understanding of the observed excitonic enhancement of optical nonlinearity via many-body calculations (Supporting Information Section 9). We first calculated the linear absorption cross-section of (6,5)⁻ CNTs via second-order perturbation theory according to Ref. [54], with the excitonic transition dipole moments evaluated using the Bethe–Salpeter equation [55]. As shown in Fig. 4a, symmetric excitonic absorption peaks are well-defined for light polarized parallel to the nanotube axis (σ_z), which is qualitatively different from previous theoretical calculations for CNT systems based on single-particle band structure (Supporting Information Section 10). Introducing a Gaussian broadening parameter $\gamma(E) = 0.07 \text{ eV} + 0.08 \text{ eV} \cdot (E - E_{11})$, which is proportional to the energy and loss channels (Supporting Information Section 9) [56], reproduces the full-width-at-half-maximum (FWHM) of the E_{11} and E_{22} excitonic peaks in the polarized

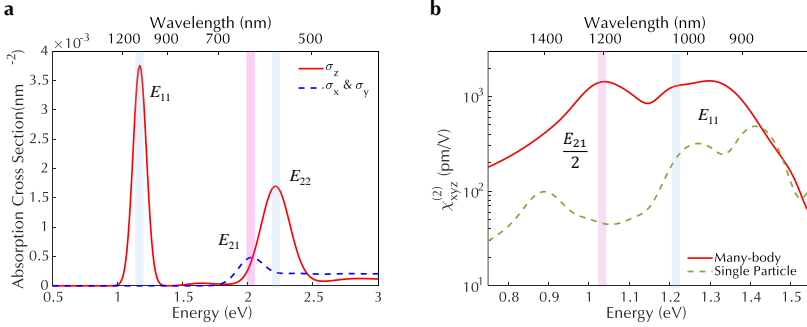


Fig. 4 Many-body atomistic calculations reproducing observed excitonic enhancement in (6,5)⁻ CNTs at E_{11}/E_{12} resonances (blue/purple shade). **(a)** Linear absorption cross section for light polarized parallel (σ_z) and perpendicular ($\sigma_{x,y}$) to the nanotube axis. **(b)** Nonlinear $|\chi_{xyz}^{(2)}|$ spectrum exhibits large enhancement over the single-particle value when using the same damping rate. The features around 0.9 eV and 1.4 eV in the single-particle calculation were not seen in the experiment, further proving the importance of many-body effects in nonlinear optical processes in CNTs.

attenuance measurements (Fig. 1f). Then, following Ref. [57], we calculated $|\chi_{xyz}^{(2)}|$ spectra with the given γ and compared the results based on the excitonic picture with those based on the single-particle picture (Fig. 4b and Supporting Information Section 9).

Without any free parameters, the calculated peak positions and values of $|\chi_{xyz}^{(2)}|$ from the excitonic picture agree with the experimental results well, in contrast to those from the single-particle calculations. The latter contains an artefact peak around 1.4 eV due to the contribution from higher-lying bands, which is a clear feature in all previous calculations but disagrees with the experiment. Another artifact around 0.9 eV is due to the incorrect energy of $E_{12} = E_{21} = (E_{11} + E_{22})/2$ whose degeneracy is lifted in the many-body picture by the exchange interaction. Previous reported $|\chi_{xyz}^{(2)}|$ values based on the single-particle picture accidentally had the right order of magnitude by using an ideal constant $\gamma = 0.05$ eV for single CNT [25, 58], as opposed to our calculation using realistic and experimentally obtained γ values for densely packed thin films (Supporting Information Section 11). Meanwhile, we note that the many-body calculation appears to overestimate the nonlinearity at E_{12} and E_{13} resonance (the feature around 1.3 eV). The fact that we did not observe a larger feature at 1.3 eV implies that the damping rate of the E_{13} transition in CNT films is larger than what we estimated in the simple model of linear energy dependence. Indeed, the E_{13} resonance was not distinguishable in the linear absorption spectrum in experiments, making it impossible to evaluate its actual γ .

In summary, we discovered giant second-order optical nonlinearity in wafer-scale, enantiomer-pure, aligned, and densely packed chiral (6,5)⁻ CNT thin

films. The dependence of the SHG emission intensity on the sample orientation and optical polarization proves that the nonlinearity originates from intrinsic structural chirality instead of extrinsic contributions such as defects and surfaces. Control experiments with randomly oriented and mixed enantiomer thin films show that alignment and enantiomer purity are crucial for the observed chirality-induced SHG. Nonlinear spectroscopy reveals two excitonic resonances at pump photon energy of 1.21 eV and 0.96 eV, which corresponds to the absorption resonance with E_{11} exciton and emission resonance with E_{12} exciton, respectively. The second-order nonlinear susceptibility tensor element $\chi_{xyz}^{(2)}$ reaches $\sim 1.5 \times 10^3$ pm/V, comparable to the highest values experimentally reported in the near-infrared, in quantitative agreement with our many-body atomistic calculations with no free parameters. Our discovery opens a route for applying wafer-scale films of chiral CNTs to nonlinear and chiral photonics. Using our synthesis method, we can fabricate wafer-scale, flexible, and micro-fabrication-compatible thin films of chiral CNTs with various enriched diameters. Possibly allowing for broadband SHG response tunability across the spectrum, from the UV to NIR range. The strong nonlinearity of the film makes it potentially a good platform for mass scale quantum circuits components [59]. Furthermore, since excitons in CNT are sensitive to external stimuli, including electrical gating [60] and dielectric screening [61], nonlinear chiral CNTs are tunable for possible optoelectronics and remote sensing.

Methods

Preparation of Enantiomer-Pure Single-Chirality (6,5)⁻ CNTs

We used enantiomer-pure single-chirality (6,5)⁻ CNTs (also known as (5,6) or (11,-5) or left-handed (6,5) CNTs), using the convention of Ref. [44]; note that Refs. [62, 63] used the opposite sign convention. In general, (n,m) CNTs are right-handed (left-handed) when $n > m$ ($n < m$), and ($n + m, -m$) CNTs are the mirror image of (n,m) CNTs [64]. They were obtained by using gel chromatography employing mixed surfactant systems [40–42]. CoMoCAT SWCNTs (704148, Sigma-Aldrich) were dispersed in 1.0% aqueous solution of sodium cholate (SC, >99%, Sigma-Aldrich) using an ultrasonicator (Sonifier 250D, Branson) with 30% output for three hours. After ultracentrifugation at 210,000g for two hours, the top 90% of the supernatant solution was collected and mixed with an aqueous solution of sodium dodecyl sulfate (SDS, >99.0%, Sigma-Aldrich) to prepare 2.0% SDS + 0.5% SC solution.

A two-step separation process using different surfactant concentrations [40] was performed automatically at 19-20 °C using a high-performance liquid chromatography system (NGC chromatography system, BIO-RAD) with columns filled with gel beads (Sephacryl S-200 HR, GE Healthcare). First, the SWCNT solution was loaded into the first column equilibrated with 2.0% SDS + 0.5% SC solution, and non-adsorbed CNTs containing (6,5) CNTs were collected as filtrate. The filtrate solution is mixed with SC solution to prepare 0.5% SDS

+ 0.5% SC solution and used for the subsequent separation process. After loading the CNT solution into the second column equilibrated with 0.5% SDS + 0.5% SC solution, adsorbed CNTs were eluted by using mixed surfactant solution containing sodium lithocholate (LC, >98%, Tokyo Chemical Industry Co., Ltd.), i.e., 0.5% SDS + 0.5% SC + x % LC solution, where x is the LC concentration increased stepwise [41].

The high-purity (6,5)- CNTs were collected by adding a gradient solution of 0.5%SDS +0.5%SC+0.029% LC solution to 0.5%SDS +0.5%SC+0.030% LC solution. For film preparation, the contained surfactants were replaced with 0.3% sodium deoxycholate (DOC) by ultrafiltration (Amicon Ultra-15 with Ultracel-100 membrane, Merck Millipore). The obtained SWCNT solution was treated with ultrasonication with 30% output for ten minutes and ultracentrifugation at 210,000g for one hour to remove aggregates and used for film preparation (CA and CR films).

CNT Thin Film Preparation

For fabricating a CA film, the enantiomer-pure (6,5)⁻ CNTs were aligned through the controlled vacuum filtration (CVF) method [46]. The mother sodium deoxycholate (DOC) suspended CNT solution was diluted apriority to filtration by pure water to reduce the concentration of DOC from 0.3% to 0.075%. A total volume of 4 mL was filtered out through the filter membrane (Whatman Nuclepore Track-Etched membranes, MilliporeSigma). The filtration occurs in three stages: the gravitational, pumping, and drying phases to maintain a high controllability over the nematic ordering of the nanotubes. After filtration, the film was transferred onto a fused silica substrate (MTI corporation) by dissolving the polycarbonate membrane with chloroform, cleaning it with isopropanol (IPA), and blowing it with dry air. For fabricating a CR film, instead of diluting the solution with pure water, 1.5 mL of CNTs suspended in DOC with 0.3% concentration was added into 8.5 mL of diluted NaSCN (10 mmol/L of Na⁺). The suspension was then filtered out at a faster pace. The fast filtration and introduction of Na⁺ into the solution help make the alignment more chaotic. For fabricating a RA film, the whole recipe can be found in our previous work [46].

Characterization of Suspension and Aligned CNT Films

Sample morphology and thickness were characterized using a scanning electron microscope (FEI APREO) and an atomic force microscope (Park Systems NX20). Enantiometric purity (EP) was evaluated by recording the CD and attenuation spectra of the suspension using a CD spectrometer (Jasco 815). The uniaxially anisotropic refractive index was extracted from the Mueller matrix spectroscopic ellipsometry data acquired at three incident angles and three azimuthal orientations using the RC2 ellipsometer setup (JA Woollam Co.Inc).

Polarized Attenuance Spectra

Polarized attenuance spectra within a μm^2 scale optically resolvable area for three samples were acquired by a home-built optical transmission measurement setup. A condensed lens was used to focus the light beam from the lamp onto the sample. The reference (transmitted) signal was collected by the objective under illumination at the area without (with) the sample. A polarizer was placed between the condenser lens and the sample to control the incident light polarization. The signal was then guided into the spectrometer through an optical fiber to get a spectrum. After subtracting noises from the spectrometer, the transmission was acquired by calculating the ratio of the transmitted spectrum over the reference spectrum. Assuming negligible reflection, attenuation was acquired by $-\log(T)$, where T is the intensity transmittance. By adjusting the magnification of the objective and the optical fiber's diameter, the probing area size can be controlled.

Polarized Raman Spectroscopy

To comprehensively analyze nematic order, we employ a state-of-the-art Raman spectroscopy technique. Operating at a pump wavelength of 532 nm, we utilized a high-resolution Raman microscope equipped with a $50\times$ objective lens, delivering a focused beam with a spot size of $1.3 \mu\text{m}^2$. To discern the alignment of nanotubes within the nematic medium, we investigated three distinct polarized configurations, VV, VH, and HH, while probing the same spot in all three configurations. The VV configuration aligned the incident and scattered light polarizations parallel to the nanotube axis, effectively probing alignment parallel to the incident beam. In the VH configuration, the incident polarization remained parallel to the nanotube axis while the scattered polarization becomes perpendicular, allowing us to gauge alignment perpendicular to the incident beam. Finally, the HH configuration employed perpendicular polarizations for both incident and scattered light. Additionally, by incorporating polarized attenuance data at 532 nm, using Equation 3, we assessed the nematic order parameter in three dimensions, which is a reasonable approximation since the thickness of the film is much larger than the diameter of the CNTs. With $\Delta = A_{\parallel}/A_{\perp}$ being the dichroic ratio [65], the nematic order parameter can be obtained as

$$S_{\text{Raman}} = \frac{6\Delta I_{\text{VV}} + 3(1 + \Delta)I_{\text{VH}} - 8I_{\text{HH}}}{6\Delta I_{\text{VV}} + 12(1 + \Delta)I_{\text{VH}} + 16I_{\text{HH}}} \quad (3)$$

Second Harmonic Generation Measurements

Second harmonic generation (SHG) measurements were performed in a transmission geometry using the home-built setup, as shown in Supplementary Information Section 12. An idler beam generated from a TOPAS Prime Automated OPA (Spectra-Physics, USA) with a 5 kHz repetition rate, a 100 fs

pulse duration, and a tunable wavelength from 1760 nm–2100 nm was used. A BBO nonlinear optical crystal was used to convert the laser wavelength to 880 nm–1050 nm via second harmonic generation, followed by a 1326 nm short pass optical filter to block the fundamental laser beam. The laser then passed through a Berek polarization compensator (Model 5540, Newport Corp.) set in half-wave plate mode to make sure the laser polarization was corrected to be in the yz ($y'z'$) plane in the laboratory (sample) coordinate system, as indicated in Fig. 2a. A convex lens with a focal length of 75 mm was utilized to focus the laser beam onto the sample. The diameter of the laser spot was measured to be around 70 μm , varying with the laser wavelength, giving a probing area on the order of $10^3 \mu\text{m}^2$. The alignment of the sample was also kept in the yz plane and tilted along the x -axis in the laboratory coordinate system so that chirality-induced SHG can be generated. The SHG signal was extracted by a 785 nm short-pass filter and a 633 nm short-pass filter. A polarizer was put right before the CMOS camera detector (PM001, Brigates Microelectronics, China) to analyze the signal's polarization. The detector recorded the SHG signal and by integrating the count from each pixel, subtracting the background, and correcting the quantum efficiency of the detector, the actual SHG photon count can be acquired.

Data Availability. Source data for the figures in the main text are provided with the paper. All other data supporting the plots within this paper and other study findings are available from the corresponding author upon reasonable request.

Acknowledgements. R.X., J.L., and H.Z. acknowledge the U.S. National Science Foundation (DMR-2240106) and Robert A. Welch Foundation (C-2128). J.D., V.L., A.B., F.T., V.P., and J.K. acknowledge the U.S. National Science Foundation (PIRE-2230727). J.D., A.B., F.T., and J.K. also acknowledge support from the Robert A. Welch Foundation (C-1509), the Air Force Office of Scientific Research (FA9550-22-1-0382), and the Chan Zuckerberg Initiative (WU-21-357). Y.Y. and K.Y. acknowledge support from JSPS KAKENHI (JP20H02573, JP21H05017, JP22H05469 and JP23H00259), JST CREST (JPMJCR17I5), and US-JAPAN PIRE collaboration (JPJSJRP20221202). W.T. and J.L. acknowledge Robert A. Welch Foundation (C-1716). EB is supported by the Graduate Research Fellowship Program (GRFP) from U.S. National Science Foundation under grant number DGE-1842494. R.S. acknowledges support from JSPS KAKENHI (JP22H00283) and Yushan Fellow Program from Taiwan.

Author Contributions. A.B., J.K., and H.Z. conceived the project. Y.Y. and K.Y. synthesized the enantiomer-pure (6,5)⁻ CNT suspension. J.D. fabricated the CNT film samples. K.Y., Y.Y., and J.D. performed circular dichroism spectroscopy. J.D. and N.H. measured the refractive index of the enantiomer-pure aligned CNT thin film. R.X., J.D., and N.H. measured the polarized attenuation spectra. J.D. and R.X. performed AFM measurements. J.D., W.T., and R.X. performed SEM measurements. J.D. performed polarized Raman

measurements. R.X. performed SHG experiments and analyzed the data. V.L. conducted the many-body atomistic calculations under the supervision of V.P. R.X., J.D., A.S., M.T.,E.B., J.L.,F.T., V.P., A.B., and H.Z. wrote the manuscript with input from all authors. All authors discussed the data.

Competing Interests. The authors declare no competing financial interests.

References

- [1] Circular Dichroism: Principles and Applications, 2nd Edition | Wiley
- [2] Ahn, J., Lee, E., Tan, J., Yang, W., Kim, B., Moon, J.: A new class of chiral semiconductors: chiral-organic-molecule-incorporating organic-inorganic hybrid perovskites. *Materials Horizons* **4**(5), 851–856 (2017)
- [3] Rikken, G.L.J.A., Raupach, E.: Observation of magneto-chiral dichroism. *Nature* **390**(6659), 493–494 (1997)
- [4] Train, C., Gheorghe, R., Krstic, V., Chamoreau, L.-M., Ovanesyan, N.S., Rikken, G.L.J.A., Gruselle, M., Verdaguer, M.: Strong magneto-chiral dichroism in enantiopure chiral ferromagnets. *Nature Materials* **7**(9), 729–734 (2008)
- [5] Naaman, R., Waldeck, D.H.: Chiral-Induced Spin Selectivity Effect. *The Journal of Physical Chemistry Letters* **3**(16), 2178–2187 (2012)
- [6] Yang, C., Li, Y., Zhou, S., Guo, Y., Jia, C., Liu, Z., Houk, K.N., Dubi, Y., Guo, X.: Real-time monitoring of reaction stereochemistry through single-molecule observations of chirality-induced spin selectivity. *Nature Chemistry*, 1–8 (2023)
- [7] Yang, Y., da Costa, R.C., Fuchter, M.J., Campbell, A.J.: Circularly polarized light detection by a chiral organic semiconductor transistor. *Nature Photonics* **7**(8), 634–638 (2013)
- [8] Brandt, J.R., Salerno, F., Fuchter, M.J.: The added value of small-molecule chirality in technological applications. *Nature Reviews Chemistry* **1**(6), 1–12 (2017)
- [9] Yang, S.-H., Naaman, R., Paltiel, Y., Parkin, S.S.P.: Chiral spintronics. *Nature Reviews Physics* **3**(5), 328–343 (2021)
- [10] Wei, Q., Ning, Z.: Chiral Perovskite Spin-Optoelectronics and Spintronics: Toward Judicious Design and Application. *ACS Materials Letters* **3**(9), 1266–1275 (2021)

- [11] Singh, S., Bonner, W.A., Van Uitert, L.G.: Violation of Kleinman's symmetry condition in paratellurite. *Physics Letters A* **38**(6), 407–408 (1972)
- [12] Chemla, D.S., Jerphagnon, J.: Optical Second-Harmonic Generation in Paratellurite and Kleinman's Symmetry Relations. *Applied Physics Letters* **20**(6), 222–223 (2003)
- [13] Yuan, C., Li, X., Semin, S., Feng, Y., Rasing, T., Xu, J.: Chiral Lead Halide Perovskite Nanowires for Second-Order Nonlinear Optics. *Nano Letters* **18**(9), 5411–5417 (2018)
- [14] Yao, L., Zeng, Z., Cai, C., Xu, P., Gu, H., Gao, L., Han, J., Zhang, X., Wang, X., Wang, X., Pan, A., Wang, J., Liang, W., Liu, S., Chen, C., Tang, J.: Strong Second- and Third-Harmonic Generation in 1D Chiral Hybrid Bismuth Halides. *Journal of the American Chemical Society* **143**(39), 16095–16104 (2021)
- [15] Ge, F., Li, B.-H., Cheng, P., Li, G., Ren, Z., Xu, J., Bu, X.-H.: Chiral Hybrid Copper(I) Halides for High Efficiency Second Harmonic Generation with a Broadband Transparency Window. *Angewandte Chemie* **134**(10), 202115024 (2022)
- [16] Boyd, R.W.: *Nonlinear Optics*. Academic Press, Boston (1992)
- [17] Cheng, M., Wu, S., Zhu, Z.-Z., Guo, G.-Y.: Large second-harmonic generation and linear electro-optic effect in trigonal selenium and tellurium. *Physical Review B* **100**(3), 035202 (2019)
- [18] Londoño-Calderon, A., Williams, D.J., Schneider, M.M., Savitzky, B.H., Ophus, C., Ma, S., Zhu, H., Pettes, M.T.: Intrinsic helical twist and chirality in ultrathin tellurium nanowires. *Nanoscale* **13**(21), 9606–9614 (2021)
- [19] Wang, H., Mao, Y., Kislyakov, I.M., Dong, N., Chen, C., Wang, J.: Anisotropic Raman scattering and intense broadband second-harmonic generation in tellurium nanosheets. *Optics Letters* **46**(8), 1812–1815 (2021)
- [20] Sherman, G., Coleman, P.: Absolute measurement of the second-harmonic generation nonlinear susceptibility of tellurium at 28.0 mm **9**(3), 403–409
- [21] Avouris, P., Freitag, M., Perebeinos, V.: Carbon-nanotube photonics and optoelectronics. *Nature Photon* **2**(6), 341–350 (2008)

- [22] Blackburn, J.L., Ferguson, A.J., Cho, C., Grunlan, J.C.: Carbon-Nanotube-Based Thermoelectric Materials and Devices. *Advanced Materials* **30**(11), 1704386 (2018)
- [23] Li, Y.: Carbon Nanotube Research in Its 30th Year. *ACS Nano* **15**(6), 9197–9200 (2021)
- [24] Baydin, A., Tay, F., Fan, J., Manjappa, M., Gao, W., Kono, J.: Carbon Nanotube Devices for Quantum Technology. *Materials*, 26 (2022)
- [25] Guo, G.Y., Chu, K.C., Wang, D.-s., Duan, C.-g.: Linear and nonlinear optical properties of carbon nanotubes from first-principles calculations. *Physical Review B* **69**(20), 205416 (2004)
- [26] Rérat, M., Karamanis, P., Civalleri, B., Maschio, L., Lacivita, V., Kirtman, B.: Ab Initio Calculation of Nonlinear Optical Properties for Chiral Carbon Nanotubes. Second Harmonic Generation and Dc-Pockels Effect. *Theor Chem Acc* **137**(2), 17 (2018)
- [27] Weisman, R.B., Kono, J.: Introduction to Optical Spectroscopy of Single-Wall Carbon Nanotubes. In: *Handbook of Carbon Nanomaterials*. World Scientific Series on Carbon Nanoscience, vol. Volume 9 & 10, pp. 1–43. World Scientific, Singapore (2017)
- [28] Nishihara, T., Takakura, A., Shimasaki, M., Matsuda, K., Tanaka, T., Kataura, H., Miyauchi, Y.: Empirical formulation of broadband complex refractive index spectra of single-chirality carbon nanotube assembly. *Nanophotonics* **11**(5), 1011–1020 (2022)
- [29] Huttunen, M.J., Herranen, O., Johansson, A., Jiang, H., Mudimela, P.R., Myllyperkiö, P., Bautista, G., Nasibulin, A.G., Kauppinen, E.I., Ahlskog, M., Kauranen, M., Pettersson, M.: Measurement of Optical Second-Harmonic Generation from an Individual Single-Walled Carbon Nanotube. *New J. Phys.* **15**(8), 083043 (2013)
- [30] Okawara, S., Kudo, M., Miyamori, M., Ohno, S., Shimazu, Y., Tanaka, M., Suzuki, T.: Second-Harmonic Generation from Supported Carbon Nanotube Films Grown by Chemical Vapor Deposition on Fused Silica. *Jpn. J. Appl. Phys.* **58**(3), 032006 (2019)
- [31] Dominicis, L.D., Fantoni, R., Botti, S., Asilyan, L.S., Ciardi, R., Fiori, A., Appolloni, R.: Symmetry point group description of second harmonic generation in carbon nanotubes. *Laser Physics Letters* **1**(4), 172 (2004)
- [32] Su, H.M., Ye, J.T., Tang, Z.K., Wong, K.S.: Resonant Second-Harmonic Generation in Monosized and Aligned Single-Walled Carbon Nanotubes. *Phys. Rev. B* **77**(12), 125428 (2008)

- [33] Murakami, Y., Kono, J.: Nonlinear Photoluminescence Excitation Spectroscopy of Carbon Nanotubes: Exploring the Upper Density Limit of One-Dimensional Excitons. *Physical Review Letters* **102**(3), 037401 (2009)
- [34] Janisch, C., Wang, Y., Ma, D., Mehta, N., Elías, A.L., Perea-López, N., Terrones, M., Crespi, V., Liu, Z.: Extraordinary Second Harmonic Generation in Tungsten Disulfide Monolayers. *Scientific Reports* **4**(1), 5530 (2014)
- [35] Kumar, N., Najmaei, S., Cui, Q., Ceballos, F., Ajayan, P.M., Lou, J., Zhao, H.: Second harmonic microscopy of monolayer MoS₂. *Physical Review B* **87**(16), 161403 (2013)
- [36] You, J.W., Bongu, S.R., Bao, Q., Panoiu, N.C.: Nonlinear optical properties and applications of 2D materials: theoretical and experimental aspects. *Nanophotonics* **8**(1), 63–97 (2019)
- [37] Kim, B., Jin, J., Wang, Z., He, L., Christensen, T., Mele, E.J., Zhen, B.: Three-dimensional nonlinear optical materials from twisted two-dimensional van der Waals interfaces. *Nature Photonics* **18**(1), 91–98 (2024)
- [38] Wu, L., Patankar, S., Morimoto, T., Nair, N.L., Thewalt, E., Little, A., Analytis, J.G., Moore, J.E., Orenstein, J.: Giant anisotropic nonlinear optical response in transition metal monpnictide Weyl semimetals. *Nature Physics* **13**(4), 350–355 (2017)
- [39] Lodahl, P., Mahmoodian, S., Stobbe, S., Rauschenbeutel, A., Schneeweiss, P., Volz, J., Pichler, H., Zoller, P.: Chiral quantum optics. *Nature* **541**(7638), 473–480 (2017)
- [40] Yomogida, Y., Tanaka, T., Zhang, M., Yudasaka, M., Wei, X., Kataura, H.: Industrial-scale separation of high-purity single-chirality single-wall carbon nanotubes for biological imaging. *Nature Communications* **7**(1), 12056 (2016)
- [41] Yomogida, Y., Tanaka, T., Tsuzuki, M., Wei, X., Kataura, H.: Automatic Sorting of Single-Chirality Single-Wall Carbon Nanotubes Using Hydrophobic Cholates: Implications for Multicolor Near-Infrared Optical Technologies. *ACS Applied Nano Materials* **3**(11), 11289–11297 (2020)
- [42] Wei, X., Tanaka, T., Hirakawa, T., Tsuzuki, M., Wang, G., Yomogida, Y., Hirano, A., Kataura, H.: High-yield and high-throughput single-chirality enantiomer separation of single-wall carbon nanotubes. *Carbon* **132**, 1–7 (2018)

- [43] Weisman, R.B., Kono, J.: Optical Properties of Carbon Nanotubes: A Volume Dedicated to the Memory of Professor Mildred Dresselhaus. World Scientific, Singapore (2019)
- [44] Wei, X., Tanaka, T., Hirakawa, T., Yomogida, Y., Kataura, H.: Determination of Enantiomeric Purity of Single-Wall Carbon Nanotubes Using Flavin Mononucleotide. *Journal of the American Chemical Society* **139**(45), 16068–16071 (2017)
- [45] Wei, X., Luo, X., Li, S., Zhou, W., Xie, S., Liu, H.: Length-Dependent Enantioselectivity of Carbon Nanotubes by Gel Chromatography. *ACS Nano* **17**(9), 8393–8402 (2023)
- [46] He, X., Gao, W., Xie, L., Li, B., Zhang, Q., Lei, S., Robinson, J.M., Háróz, E.H., Doorn, S.K., Wang, W., Vajtai, R., Ajayan, P.M., Adams, W.W., Hauge, R.H., Kono, J.: Wafer-scale monodomain films of spontaneously aligned single-walled carbon nanotubes. *Nature Nanotechnology* **11**(7), 633–638 (2016)
- [47] Maultzsch, J., Telg, H., Reich, S., Thomsen, C.: Radial breathing mode of single-walled carbon nanotubes: Optical transition energies and chiral-index assignment. *Phys. Rev. B* **72**, 205438 (2005)
- [48] Katsutani, F., Gao, W., Li, X., Ichinose, Y., Yomogida, Y., Yanagi, K., Kono, J.: Direct observation of cross-polarized excitons in aligned single-chirality single-wall carbon nanotubes. *Physical Review B* **99**(3), 035426 (2019)
- [49] Qian, H., Li, S., Chen, C.-F., Hsu, S.-W., Bopp, S.E., Ma, Q., Tao, A.R., Liu, Z.: Large optical nonlinearity enabled by coupled metallic quantum wells. *Light: Science & Applications* **8**(1), 13 (2019)
- [50] Fu, Q., Cong, X., Xu, X., Zhu, S., Zhao, X., Liu, S., Yao, B., Xu, M., Deng, Y., Zhu, C., Wang, X., Kang, L., Zeng, Q., Lin, M.-L., Wang, X., Tang, B., Yang, J., Dong, Z., Liu, F., Xiong, Q., Zhou, J., Wang, Q., Li, X., Tan, P.-H., Tay, B.K., Liu, Z.: Berry Curvature Dipole Induced Giant Mid-Infrared Second-Harmonic Generation in 2D Weyl Semiconductor. *Advanced Materials* **35**(46), 2306330 (2023)
- [51] Zhang, Y., Gao, B., Lepage, D., Tong, Y., Wang, P., Xia, W., Niu, J., Feng, Y., Chen, H., Qian, H.: Large second-order susceptibility from a quantized indium tin oxide monolayer. *Nature Nanotechnology*, 1–8 (2024)
- [52] Hussain, S.A.: Comparison of Graphene and Carbon Nanotube Saturable Absorbers for Wavelength and Pulse Duration Tunability. *Scientific Reports* **9**(1), 17282 (2019)

- [53] Wang, J., Liang, X., Hu, G., Zheng, Z., Lin, S., Ouyang, D., Wu, X., Yan, P., Ruan, S., Sun, Z., Hasan, T.: 152 fs nanotube-mode-locked thulium-doped all-fiber laser. *Scientific Reports* **6**(1), 28885 (2016)
- [54] Malapanis, A., Perebeinos, V., Sinha, D.P., Comfort, E., Lee, J.U.: Quantum efficiency and capture cross section of first and second excitonic transitions of single-walled carbon nanotubes measured through photoconductivity. *Nano Letters* **13**, 3531–3538 (2013)
- [55] Rohlfing, M., Louie, S.G.: Electron-hole excitations and optical spectra from first principles. *Phys. Rev. B* **62**, 4927–4944 (2000)
- [56] Hertel, T., Perebeinos, V., Crochet, J., Arnold, K., Kappes, M., Avouris, P.: Intersubband decay of 1-d exciton resonances in carbon nanotubes. *Nano Letters* **8**, 87–91 (2008)
- [57] Boyd, R.W. (ed.): *Nonlinear Optics (Fourth Edition)*. Academic Press, London (2020)
- [58] Pedersen, T.G., Pedersen, K.: Systematic tight-binding study of optical second-harmonic generation in carbon nanotubes. *Physical Review B* **79**(3), 035422 (2009)
- [59] Guo, Q., Qi, X.-Z., Zhang, L., Gao, M., Hu, S., Zhou, W., Zang, W., Zhao, X., Wang, J., Yan, B., Xu, M., Wu, Y.-K., Eda, G., Xiao, Z., Yang, S.A., Gou, H., Feng, Y.P., Guo, G.-C., Zhou, W., Ren, X.-F., Qiu, C.-W., Pennycook, S.J., Wee, A.T.S.: Ultrathin quantum light source with van der Waals NbOCl₂ crystal. *Nature* **613**(7942), 53–59 (2023). <https://doi.org/10.1038/s41586-022-05393-7>
- [60] Chernikov, A., van der Zande, A.M., Hill, H.M., Rigosi, A.F., Velauthapillai, A., Hone, J., Heinz, T.F.: Electrical Tuning of Exciton Binding Energies in Monolayer WS₂. *Physical Review Letters* **115**(12), 126802 (2015)
- [61] Lin, Y., Ling, X., Yu, L., Huang, S., Hsu, A.L., Lee, Y.-H., Kong, J., Dresselhaus, M.S., Palacios, T.: Dielectric Screening of Excitons and Trions in Single-Layer MoS₂. *Nano Letters* **14**(10), 5569–5576 (2014)
- [62] Ghosh, S., Bachilo, S.M., Weisman, R.B.: Advanced sorting of single-walled carbon nanotubes by nonlinear density-gradient ultracentrifugation. *Nature Nanotechnology* **5**(6), 443–450 (2010)
- [63] Ao, G., Streit, J.K., Fagan, J.A., Zheng, M.: Differentiating Left- and Right-Handed Carbon Nanotubes by DNA. *Journal of the American Chemical Society* **138**(51), 16677–16685 (2016). Publisher: American Chemical Society

- [64] Samsonidze, G.G., Grüneis, A., Saito, R., Jorio, A., Souza Filho, A.G., Dresselhaus, G., Dresselhaus, M.S.: Interband optical transitions in left- and right-handed single-wall carbon nanotubes. *Phys. Rev. B* **69**, 205402 (2004)

- [65] Zamora-Ledezma, C., Blanc, C., Maugey, M., Zakri, C., Poulin, P., Anglaret, E.: Anisotropic Thin Films of Single-Wall Carbon Nanotubes from Aligned Lyotropic Nematic Suspensions. *Nano Letters* **8**(12), 4103–4107 (2008)